A simplified algorithm to solve optimal power flows in hybrid VSC-based AC/DC systems

Javier Renedo, Ahmad Asrul Ibrahim, Behzad Kazemtabrizi, Aurelio García-Cerrada, Luis Rouco,
Quanyu Zhao and Javier García-González (*)

Abstract

High Voltage Direct Current systems based on Voltage Source Converters (VSC-HVDC) are increasingly being considered as a viable technology with advantages, above all when using underground or submarine cables for bulk power transmission. In order to fully understand how VSC-HVDC systems can be best used within existing power systems, it is necessary to adapt conventional tools to carry out system-wide studies including this technology. Along this line, this paper proposes a simplified algorithm to solve optimal power flows (OPFs) in hybrid VSC-based Alternating Current / Direct Current (AC/DC) grids with multi-terminal VSC-HVDC systems. The proposed algorithm makes it possible to seamlessly extend a previous large-scale AC case to which several multi-terminal VSC-HVDC systems must be added. The proposed approach combines two ideas used previously in two different modelling approaches: each VSC is modelled as two generators with a coupling constraint; and DC grids are modelled as notional AC grids, since, in per unit, the equations for the former are a particular case of the latter with resistive lines and no reactive-power injections. In the proposed approach, the hybrid VSC-based AC/DC system is transformed into an equivalent only-AC system. Therefore, the OPF solution of the AC/DC system can be found with the same tool used for the previous AC problem and a simple extension of the original case.

Index Terms

VSC HVDC, HVDC transmission, multi-terminal, optimal power flow, power systems.

NOMENCLATURE

A_G, A_{bus}, A_{branch}, A_{slacks} : Sets of the generators, buses, branches and slack buses of the AC grids, respectively.

A_{vsc}, A_{dcbus}, $A_{dcbranch}$: Sets of the VSC stations, buses and branches of the multi-terminal VSC-HVDC systems.

$\bar{V}_i = V_i \angle \theta_i$: Voltage at AC bus i

$\bar{S}_{G,i} = P_{G,i} + jQ_{G,i}$: Active-(P) and reactive-power (Q) generation (bus i)

$\bar{S}_{D,i} = P_{D,i} + jQ_{D,i}$: P/Q consumed by the loads (bus i)

$\bar{S}_i = P_i + jQ_i$: P/Q injections into the AC grid at bus i

$\bar{Y}_{bus,ik} = G_{ik} + jB_{ik}$: Admittance matrix of AC line (i,k)

I_{ik} : Current through AC branch (i,k) (leaving bus i) (magnitude)

$\bar{S}_{ik} = P_{ac,ik} + jQ_{ac,ik}$: P and Q flows through AC branch (i,k) (leaving AC bus i)

$\bar{Z}_{ac,ik} = R_{ac,ik} + jX_{ac,ik}$: Series impedance of AC branch (i,k)

$B_{ac,sh,ik}$: Shunt susceptance of AC branch (i,k)

$\bar{V}_{s,i} = V_{s,i} \angle \delta_{s,i}$: AC voltage at the PCC of VSC i

$\bar{E}_{c,i} = E_{c,i} \angle \delta_{c,i}$: Output AC voltage of VSC i

m_i : Modulation index of VSC i (p.u.)

$\bar{S}_{s,i} = P_{s,i} + jQ_{s,i}$: P and Q injections of VSC i at the PCC

$\bar{S}_{c,i} = P_{c,i} + jQ_{c,i}$: Output P and Q injections of VSC i

$I_{s,i}$: AC current of VSC i (magnitude)

$\bar{Z}_{s,i} = R_{s,i} + jX_{s,i}$: Connection impedance of VSC i to the PCC (phase reactor + transformer)

$P_{loss,i}$: Losses of VSC i

$P_{dc,i}$, $I_{dc,i}$: Power and current injection at DC bus i, respectively

$V_{dc,i}$: Voltage at DC bus i

$P_{cc,ik}$, $I_{cc,ik}$: Power and current flow through DC branch (i,k) (leaving DC bus i), respectively

$R_{dc,ik}$: Resistance of DC branch (i,k)

I. INTRODUCTION

Optimal Power Flow (OPF) calculations determine an optimal operating point of a power system with respect to an objective function (economical or technical) subject to grid and operation constraints, and it has long become an essential tool for Transmission System Operators (TSOs) [1]. Point-to-point high voltage direct current links based on thyristors (LCC-HVDC) are already common elements in power transmission system analysis and planning but more recently, plans to build multi-terminal HVDC grids based on Voltage Source Converters (VSC-HVDC) are emerging in the European context [2]. Along this line, TSOs demand appropriate OPF tools for the operation and planning of those hybrid HVAC/VSC-HVDC grids (HVAC refers to High Voltage Alternating Current systems).

Several OPF algorithms have been proposed for VSC-based hybrid AC/DC systems in the last few years [3]–[14] with two main distinctive elements with respect to their only-AC counterparts:

- Modelling aspects: inclusion of the equations of the VSC stations, the DC grids and the AC/DC coupling into the optimisation problem.
- Optimisation variables: active- (P) and reactive-power (Q) injections by the VSCs are control variables in the optimisation problem.

The work in [3]–[5], [7], [9], [11] presented the guidelines for modelling VSC-HVDC multi-terminal systems (VSC-MTDC, for short) in OPF problems. Those algorithms have been used succesfully for a wide range of applications in VSC-based AC/DC systems, such as minimisation of generation costs [3], [4], [14], minimisation of system losses [5], [11], [15], analysis of different objective functions [9], cost-benefit analysis of VSC-MTDC installations with different topologies [7], optimal operation in multi-area systems with different TSOs [8], [10], [16], analysis of the impact of VSC losses on OPF solutions [13] and optimisation in active distribution grids [17], among others. Meanwhile, several security-constrained OPF models for hybrid AC/DC systems were proposed in [6], [12], [18]–[21].

Regarding the modelling approach used, OPF algorithms for hybrid AC/DC systems published so far can be classified into two types, that will be referred in this paper as type-1 [4]–[14] and type-2 [3], [17], [22]–[24] models. Both approaches differ in the way in which VSC stations and DC grids are modelled. In type 1, DC grids are represented by their DC power-flow equations and each VSC station is represented as two generators (one connected to the AC side and the other one connected to the DC side) which are coupled by power conservation principle. Meanwhile, in type 2, DC grids are represented as notional AC grids: the DC lines are modelled as resistive AC lines (with null reactance), based on the fact that, in per unit, the power-flow equations of a DC grid can be thought of as a special case of an AC grid with resistive lines and no reactive-power injections. Meanwhile, VSC stations are modelled as complex-tap changing transformers. Two constraints are added to each VSC station, one to ensure that the angle of the transformer is equal to the angle of the internal AC voltage of the VSC and another one to ensure that no reactive power is injected by the VSC station into the DC side.

Although the formulation of OPF problems in hybrid AC/DC systems been reported in the literature [3]–[14], [17], [23], the implementation of either type 1 or type 2 models in only-AC OPF tools is often troublesome (or even impossible) due to lack of flexibility in those tools.

In type-1 models the power-flow equations of DC grids have to be included using equations different from those used for AC grids. Since type-2 models represent DC grids as notional AC grids, power-flow equations of the model do not need to be modified. However, equations of those complex-tap changing transformers that model VSC stations must be adapted accordingly, by introducing additional constraints.

In general, industry is very reluctance to use any new software for power system analysis. Among other reasons, this is probably due to (a) their interest on dealing with large-scale cases they had already been using for some time and (b) the experience already acquired by their personnel on the software used. Therefore, not having to modify any previously-built cases is seen as an important implementation advantage. The current situation dominated by large AC power systems with many OPF study cases already fully tested with software packages such as PSS/E [25] or PowerFactory [26] raises the question of whether one can easily add, as a plug-in, a VSC-MTDC system without having to write the whole problem from scratch. While this is not possible using either type-1 or type-2 models, the main contribution of this paper is the proposal of a simple and unified algorithm to solve an OPF problem in a hybrid AC/DC system with several VSC-MTDC systems starting from an existing only-AC case and using the same traditional only-AC tool. To achieve this, it is necessary to combine the ideas of type-1 and type-2 models for hybrid AC/DC systems. In the methodology proposed, each VSC station is modelled as two coupled AC sources

(as in type-1 models): one connected to the AC grid and the other one connected to the DC grid, which is modelled as a notional AC grid, representing the DC lines as resistive AC lines (as in type-2 models). Each VSC station also needs a constraint equation to relate active power injections of the AC and DC sides taking converter losses into account. Since converter losses are best represented by a nonlinear equation of the AC current [27], a linear approximation of those losses at the operating point has been used and an additional iteration to calculate the operating point for the converter current has been implemented to maintain a reasonable accuracy.

This paper describes how the VSC stations and the DC grids are modelled, the OPF problem formulation and the implementation of the proposed algorithm in an only-AC OPF tool. A comparison of the results with two algorithms already published is also detailed.

The rest of the paper is organised as follows. Section II describes OPF formulation for conventional AC systems. Section III presents the guidelines of steady-state modelling of hybrid VSC-based AC/DC systems for power-flow and OPF calculation, classifying current approaches into type-1 and type-2 models. Section IV presents the proposed OPF model for hybrid VSC-based AC/DC systems. Section V presents the validation of the proposed approach against two different OPF algorithms based on type 1 and 2 models used in previous publication. For this validation the Stagg's 5-bus test system with an embedded VSC-MTDC system has been used because it is reasonably small and it is well documented in the literature. Section VI presents the validation of the proposed approach in a larger system against an OPF algorithm (type 1 model) used in a previous publication. The IEEE 30-bus test system with two embedded VSC-MTDC systems has been used. Section VII presents the OPF results obtained with the proposed algorithm in a third case study (Cigré Nordic32A test system with an embedded VSC-MTDC system). This last system is specially useful to illustrate the advantages of power transmission with VSC-HVDC systems. Finally, Section VIII presents the conclusions of the paper.

II. OPF FOR AC SYSTEMS

The solution of the OPF of an arbitrary AC system, typically, minimises the generation costs and is formulated as follows:

$$\min \sum_{i \in A_G} (c_{a,i} + c_{b,i} P_{G,i} + c_{c,i} P_{G,i}^2) \tag{1}$$

s. t.

$$P_{G,i} - P_{D,i} - P_i = 0, \ \forall i \in A_{bus} \tag{2}$$

$$Q_{G,i} - Q_{D,i} - Q_i = 0, \ \forall i \in A_{bus} \tag{3}$$

$$\theta_i = 0, \ \forall i \in A_{slacks} \tag{4}$$

$$V_i^{min} \le V_i \le V_i^{max}, \ \forall i \in A_{bus} \tag{5}$$

$$P_{G,i}^{min} \le P_{G,i} \le P_{G,i}^{max}, \ \forall i \in A_G \tag{6}$$

$$Q_{G,i}^{min} \le Q_{G,i} \le Q_{G,i}^{max}, \ \forall i \in A_G \tag{7}$$

$$0 \le I_{ik} \le I_{ik}^{max}, \ \forall (i,k) \in A_{branch} \tag{8}$$

where the active- (P) and reactive-power (Q) injections into the AC grid at bus i (power-flow equations) are given by:

$$P_i = V_i \sum_{k \in A_{bus}} V_j (G_{ik} \cos \theta_{ik} + B_{ik} \sin \theta_{ik}), \tag{9}$$

$$Q_i = V_i \sum_{k \in A_{bus}} V_j (G_{ik} \sin \theta_{ik} - B_{ik} \cos \theta_{ik}), \tag{10}$$

and $\theta_{ik} = \theta_i - \theta_k$.

All variables in (1)-(10) are described in the Nomenclature Section, at the beginning of the paper. The objective function (generation costs) of the OPF is (1). Equality constraints in (2)-(3) are the power-balance equations for each bus, while equality constraints in (4) set the voltage angles of the slack buses to zero (there can be more than one slack bus if the system contains asynchronous AC areas). Inequality constraints in (5)-(8) represent voltage limits, P-Q capabilities of generators and thermal limits of AC lines.

III. Hybrid VSC-based AC/DC systems

Figure 1 depicts a hybrid AC/DC system with multi-terminal VSC-HVDC systems and Fig. 2 shows the single-line diagram of a VSC station (in per unit system). The connection impedance $\bar{Z}_{s,i} = R_{s,i} + jX_{s,i}$ represents the transformer and the phase reactor of the VSC station. It is assumed that the HVDC system has symmetrical monopole configuration (see the Appendix section). Each VSC station is connected to an AC grid and to a DC grid. The active-power injections at the AC and DC sides of the VSCs are coupled by (Fig. 2):

$$P_{c,i} + P_{dc,i} + P_{loss,i} = 0 \tag{11}$$

Losses of every VSC-i in (11) can be calculated using a quadratic model as proposed in [27]:

$$P_{loss,i} = a_i + b_i \cdot I_{s,i} + c_i \cdot I_{s,i}^2 \tag{12}$$

where $I_{s,i}$ is the current injected at the AC side by VSCi.

The magnitude of the output AC voltage ($E_{c,i}$) and the DC voltage ($V_{dc,i}$) of a VSC station verify:

$$E_{c,i} = m_i V_{dc,i}, \ 0 \leq m_i \leq m_i^{max} \tag{13}$$

where m_i is the modulation index in p.u. The maximum modulation index can be found in [28], [29], and written in per unit reads:

$$m_i^{max} = \sqrt{\frac{3}{2}} \cdot \frac{V_{dc,B}}{V_{ac,B}} \ \text{(p.u.)} \tag{14}$$

where $V_{dc,B}$ is the nominal DC voltage (pole to ground, of a symmetrical monopole) used as DC-voltage base value and $V_{ac,B}$ is the nominal AC voltage (phase to phase) used as AC-voltage base value (see the Appendix for details of the per unit system used).
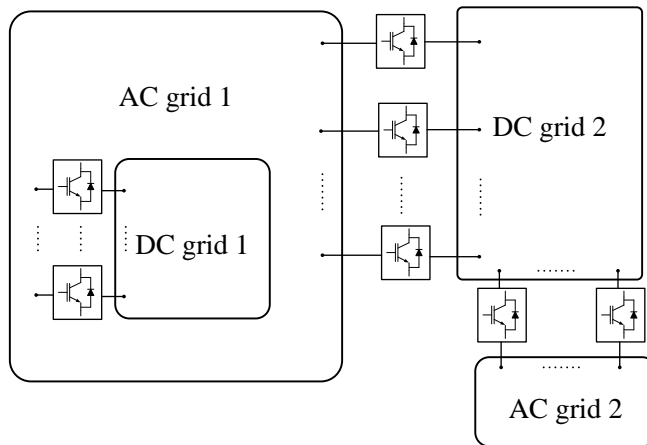

Fig. 1: Hybrid AC/DC grid based on VSCs.

Converters have two degrees of freedom for control: each VSC station can control (a) its active-power injection into the AC grid ($P_{s,i}$) or its DC voltage ($V_{dc,i}$) and (b) its reactive-power injection into the AC grid ($Q_{s,i}$) or the magnitude of the AC voltage at the connection point ($V_{s,i}$). Meanwhile, each DC grid will have one DC-slack converter that controls its DC voltage.

The modelling approach used for VSC stations and DC grids in type-1 and type-2 approaches are briefly described in this section, since those ideas will be combined and used for the proposed OPF algorithm presented in Section IV.
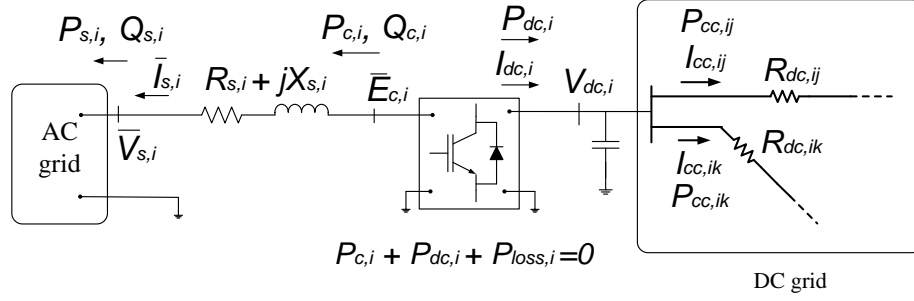
Fig. 2: VSC station.

A. Type-1 models

The guidelines of type-1 steady-state models for power-flow calculation have been describedin different publications for point-to-point [28], [30], [31] and multi-terminal [4], [32]–[43] VSC-HVDC systems. The same modelling philosophy has been used for OPF calculation of hybrid VSC-based AC/DC systems [4]–[14].

In type-1 models, VSC stations are seen as generators from, both, the AC and the DC sides, and their P injections are coupled by constraint (11), as shown in Fig. 3a. Furthermore, specific power-flow equations of DC grids are included very much in the same way as AC power-flow equations. In DC grids, voltages are real numbers and there is no reactive power, which simplifies power-flow equations in comparison with typical AC systems. Power flow through a generic DC line $i - k$, leaving DC bus i (see Fig. 2), is given by:

$$P_{cc,ik} = \frac{V_{dc,i}}{R_{dc,ik}}(V_{dc,i} - V_{dc,k}) \tag{15}$$
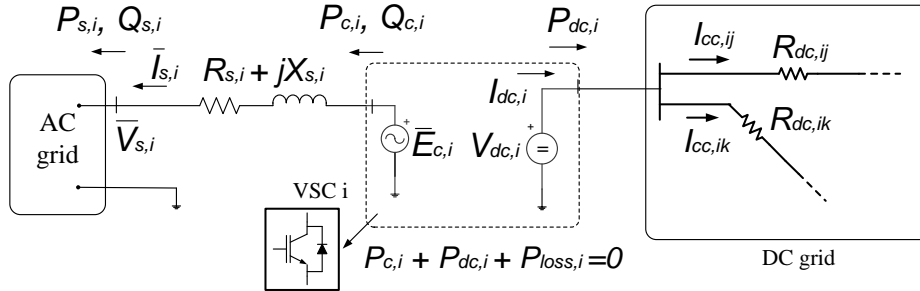
(a) Type-1 model
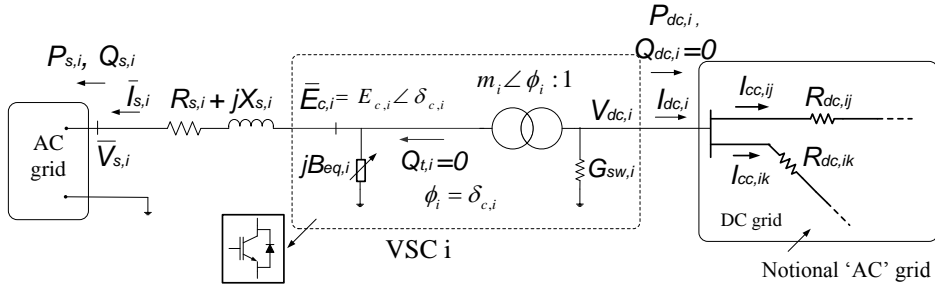
(b) Type-2 model

Fig. 3: Hybrid VSC-based AC/DC system.

B. Type-2 models

Type-2 steady-state models for hybrid VSC-based AC/DC systems were proposed in [3], [22], [24], [44] and have been used to incorporate models of STATCOMs [23], point-to-point [3], back-to-back [17] and multi-terminal [3] VSC-HVDC systems into OPF problems.

In type-2 models, VSC stations are modelled as complex-tap changing transformers and the DC grids are represented as notional AC grids (i.e with resistive AC lines), as shown in Fig. 3b. Therefore, identical power-flow equations are used for the AC and DC grids and VSCs are treated as branch devices. The angle of the complex-tap of the transformer that models each VSC must be equal to the angle of the AC voltage of each VSC ($\bar{E}_{c,i}$): $\phi_i = \delta_{c,i}$. Converter losses are prepresented by a variable shunt conductance (see Fig. 3b) proportional to the square of the AC current of the VSC ($G_{sw,i}$) [17], [22], [23]:

$$P_{loss,i} = G_{sw,i}V_{dc,i}^2, \ \ G_{sw,i} = G_{0,i}I_{s,i}^2. \tag{16}$$

An additional variable susceptance ($B_{eq,i}$) is used to ensure zero Q injection into the DC grid (see Fig. 3b). The constraint that ensures $Q_{dc,i} = 0$ at each VSC is given by [17], [22], [23]:

$$Im\{G_{sw,i}V_{dc,i}^2 + (\bar{Y}_{m,i}^* - jB_{eq,i})m_i^2 V_{dc,i}^2 - m_i e^{j\phi_i}\bar{Y}_{m,i}^* V_{dc,i}\bar{V}_{s,i}^*\} = 0 \tag{17}$$

where $\bar{Y}_{m,i}$ is defined as:

$$\bar{Y}_{m,i} = \frac{R_s - jX_s}{R_s^2 + X_s^2} \tag{18}$$

DC grids can be represented as AC grids because the power-flow equations (written in p.u) of the former are a particular case of the power-flow equations of the latter. One can go from an AC line to a DC line (Fig. 4) if:

$$V_i = V_{dc,i}, \ \ V_k = V_{dc,k}, \ \ \theta_i = \theta_k = 0, \tag{19}$$

$$\bar{Z}_{ac,ik} = R_{dc,ik} + j0, \ \ B_{ac,sh,ik} = 0. \tag{20}$$

with the terms of the admittance matrix of the AC line being $G_{ik} = -1/R_{dc,ik}$ and $B_{ik} = 0 \ \forall i,j$. Condition (20) will be imposed by modelling DC lines as AC lines with resistances only, while condition (19) is a consequence of the modelling approach: in an AC grid with only-resistive lines and with active-power injections, but without reactive-power injections, all bus voltages will have the same angle, always.

Therefore, the power flow through AC and DC lines have the same expression:

$$\begin{aligned} P_{ac,ik} &= V_i V_k (G_{ik}\cos\theta_{ik} + B_{ik}\sin\theta_{ik}) - G_{ik}V_i^2 \\ &= \frac{V_{dc,i}}{R_{dc,ik}}(V_{dc,i} - V_{dc,k}) = P_{cc,ik} \end{aligned} \tag{21}$$

$$Q_{ac,ik} = V_i V_k (G_{ik}\sin\theta_{ik} - B_{ik}\cos\theta_{ik}) + (B_{ik} - \frac{B_{ac,sh,ik}}{2})V_i^2 = 0 \tag{22}$$
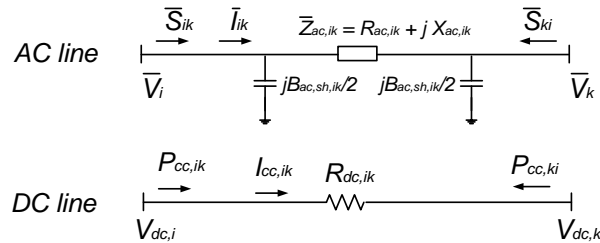

Fig. 4: AC and DC lines.

and power-flow equations of an AC system need not be modified to include DC grids when formulating an OPF problem.

IV. Proposed algorithm for OPF calculation of hybrid VSC-based AC/DC systems

A. Modelling approach

The simplified approach proposed is this work is shown in Fig. 5 (type 3, for short). It combines ideas of types 1 and 2, to ease the implementation. VSC stations and the DC grids are modelled in such way that the AC/DC OPF can be written as an only-AC OPF (1)-(8). Therefore, a conventional OPF tool only valid for AC systems could be used to solve an OPF of a hybrid VSC-based AC/DC system.

The algorithm can be summarised as follows:

- AC grids are modelled as usual and the VSC stations are seen by the AC grids as generators (as in type-1 models [4]–[14], [16]).
- DC grids are modelled as notional AC grids with resistive lines (as in type-2 models [3], [17], [22]–[24]) and VSC stations are seen by the notional AC grids as conventional AC generators.
- A linear constraint is added for each VSC station, to ensure energy conservation in the VSCs. This constraint is obtained by linearising (11), as proposed in [14]. The purpose is to obtain a linear constraint as a function of the active-power injections at AC and DC sides, which are state variables of the optimisation problem. This constraint can be implemented easily.
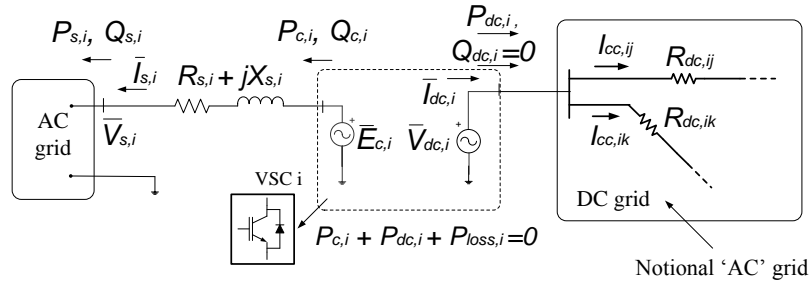

Fig. 5: Proposed OPF algorithm for AC/DC grids.

Operating limits of VSCs and voltage and thermal limits in DC grids are given by (see [9], for example):

$$P_{c,i}^{min} \leq P_{c,i} \leq P_{c,i}^{max}, \ \forall i \in A_{vsc} \tag{23}$$

$$Q_{c,i}^{min} \leq Q_{c,i} \leq Q_{c,i}^{max}, \ \forall i \in A_{vsc} \tag{24}$$

$$0 \leq I_{s,i} \leq I_{s,i}^{max}, \ \forall i \in A_{vsc} \tag{25}$$

$$0 \leq E_{c,i} \leq m_i^{max} V_{dc,i}, \ \forall i \in A_{vsc} \tag{26}$$

$$V_{dc,i}^{min} \leq V_{dc,i} \leq V_{dc,i}^{max}, \ \forall i \in A_{dcbus} \tag{27}$$

$$0 \leq |I_{cc,ik}| \leq I_{cc,ik}^{max}, \ \forall i \in A_{dcbranch} \tag{28}$$

P and Q limits of VSC stations (at the AC side) are included in the model as P and Q limits of conventional generators ((6) and (7), respectively); current limits of the VSCs are represented as current limits of AC branches (8). Meanwhile, voltage limits of DC buses and current limits of DC lines are included as voltage and current limits at buses and through branches, respectively, of the notional AC grids: (5) and (8), respectively. Maximum output voltage of a VSC depends on maximum modulation index (m_i^{max}) and its DC voltage ($V_{dc,i}$) (constraint (26)). Initially, this limit is approximated by assuming a nominal DC voltage ($V_{dc,i} = 1$ p.u.):

$$0 \leq E_{c,i} \leq E_{c,i}^{max} = m_i^{max}, \ \forall i \in A_{vsc} \tag{29}$$

The exact constraint imposed by the maximum modulation index (26) will be implemented by using an external iteration, which will be presented in Section IV-B.

Every DC grid will have a slack bus (n_s) that will set its voltage angle to zero: $\theta_{dc,n_s} = 0$, using constraint (4). Since converters will not inject reactive power into DC grids ($Q_{dc,i} = 0$, see Fig. 6) and branches of DC grids are resistive, the voltage angle of DC buses other than the slack will also be zero: $\theta_{dc,i} = 0, \forall i \in A_{dcbus}$. Notice that there is no need to add a constraint to ensure $Q_{dc,i} = 0$, because, since there will be nothing such as Q

generation/consumption in the notional AC grids, the optimal solution will always produce $Q_{dc,i} = 0$, to reduce ohmic losses and therefore to reduce generation costs.

The general model of the converter losses in (12) is a non-linear function of the converter AC current ($I_{s,i}$). Constraints that are linear functions of the state variables of the OPF are the ones that are easier to implement. Constraint (12) is also a non-linear function of the active-power injection of the converter ($P_{c,i}$), which is a state variable of the optimisation problem, and needs further manipulation before (11) can be used as a linear constraint coupling the AC and DC sides. Using $x_i = I_{s,i}^2$ in (12), as suggested in [14], converter losses are:

$$P_{loss,i} = a_i + b_i \cdot \sqrt{x_i} + c_i \cdot x_i \tag{30}$$

where, $\sqrt{x_i}$ can be linearised around an operating point:

$$\sqrt{x_i} \simeq \sqrt{x_i^0} + \left(\frac{1}{2\sqrt{x_i^0}}\right)(x_i - x_i^0), \tag{31}$$

Replacing (31) in (30) and undoing the change of variable:

$$P_{loss,i} \simeq \left(a_i + \frac{b_i I_{s,i}^0}{2}\right) + \left(c_i + \frac{b_i}{2I_{s,i}^0}\right) I_{s,i}^2 \tag{32}$$

Quadratic coefficients c_i and $b_i/(2I_{s,i}^0)$ can be modelled as resistances ($R_{loss,c,i} = c_i$ and $R_{loss,b,i} = b_i/(2I_{s,i}^0)$, respectively) by adding a ficticious branch [14], as shown in Fig. 6. Hence, the equation of power balance at each VSC station (11) can be written now as a linear constraint relating the active-power injections at both sides of each VSC:

$$P'_{c,i} + P_{dc,i} + a_i + \frac{b_i I_{s,i}^0}{2} = 0 \tag{33}$$

Notice that if $I_{s,i}^0 = 0$, the linearisation is not needed since converter losses would be $P_{loss,i} = a_i$.
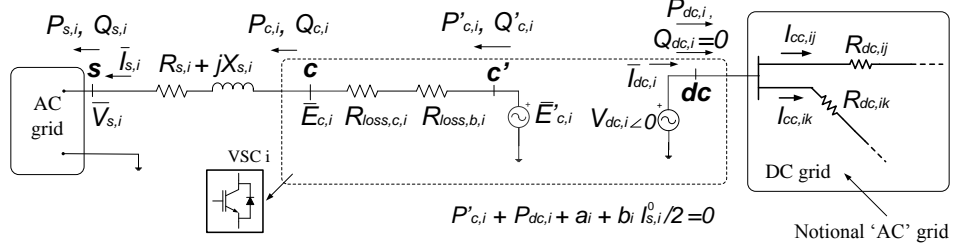

Fig. 6: VSC station: ficticious branch $c - c'$.

Since the generator that models the AC side of a VSC i will be connected to fictitious bus ci' instead of bus ci (Fig. 6), a correction for the active-power limits in (23) is required:

$$P_{c,i}^{corr,max} = P_{c,i}^{max} + \gamma_i (R_{loss,b,i} + R_{loss,c,i})(I_{s,i}^0)^2 \tag{34}$$

$$P_{c,i}^{corr,min} = P_{c,i}^{min} + \gamma_i (R_{loss,b,i} + R_{loss,c,i})(I_{s,i}^0)^2 \tag{35}$$

where $\gamma_i = 1$ if $P_{c,i} \geq 0$ and $\gamma_i = -1$ if $P_{c,i} < 0$. Parameter γ_i is fixed for each OPF solution and it is only updated for each external iteration (IV-B).

Notice that the approximation of (31) depends on the current of the VSC at the operating point, which is indeed an unknown of the problem. To start with, a current obtained from a previous solution could be used, or $I_{s,i}^0 = 0$, if starting from scratch. Although the effect of having this inaccuracy in the model of the converter losses may have a small impact on the OPF solution, it would be desirable to be able to use the exact loss value in VSC stations. The way in which this problem has been tackled is explained in Section IV-B.

After these modifications, the resulting AC/DC system will contain asynchronous AC grids only (true AC grids + notional AC grids in place of the DC grids) with some extra constraints coupling some generators of each of the two systems (those that model the VSCs). Therefore, a conventional only-AC OPF problem (1)-(8) with the additional linear constraints provided by (33) can now be solved.

B. External iteration to improve the accuracy of the algorithm

The final algorithm has been implemented with an external iteration, to take into account the exact loss value and the exact maximum modulation index of every VSC station:

1) Make $k = 0$ and choose an initial guess for the currents of VSCs at the operating point ($I_{s,i}^0(k = 0)$ in (32)). Choose $I_{s,i}^0(k = 0) = 0$ if there is no clue about the current values. Choose an initial guess for the maximum output AC voltage of the converter: $E_{c,i}^{max}(k = 0) = m_i^{max}$.
2) Solve the AC/DC OPF problem using the algorithm described in Subsection IV-A, using $I_{s,i}^0(k)$.
3) Use the DC voltage obtained from the OPF ($V_{dc,i}(k)$) and the maximum modulation index ($m_{max,i}$) to compute the true maximum output AC voltage for each converter i: $E_{c,i}^{max}(k + 1) = m_i^{max}V_{dc,i}(k)$ in (29).
4) Use the current obtained from the OPF in $I_{s,i}^0(k + 1)$), for each converter i.
5) Convergence test: If $\max_i\{|I_{s,i}^0(k + 1) - I_{s,i}^0(k)|, |E_{c,i}^{max}(k + 1) - E_{c,i}^{max}(k)|\} < \epsilon$: stop and if not, make $k = k + 1$ and return to step 2.

With this iteration, the proposed simplified model captures all details of state-of-the-art OPF models for hybrid VSC-based AC/DC systems.

C. Implementation

The proposed OPF algorithm has been implemented in Matpower [45], which is a Matlab-based open-source tool for power flow and optimal power flow calculation of AC systems, but it cannot deal with AC/DC systems. The algorithm described in Subsections IV-A and IV-B has been implemented in Matlab scripts which manipulate the input data and call Matpower to solve the OPF of the resulting equivalent only-AC system. The linear equality constraints in (33) have been implemented in Matpower following the guidelines of [46].

MatACDC [47] is another open-source tool based on Matlab + Matpower for power-flow calculation of hybrid AC/DC systems, but it cannot solve optimal power flows. MatACDC extended the comprehensive data format of Matpower for AC/DC grids. To take advantage of this structure of the input data, the OPF tool developed in this work and implemented in Matpower has been linked with MatACDC. In this way, the input data will be in MatACDC format and at the end of the algorithm described in Subsection IV-B a power flow is solved with MatACDC, aiming to have the resulting operating point in MatACDC format and use it for other steady-state studies with that tool, if desired.

Finally, the requirements for the implementation of the proposed algorithm are summarised below:

1) The tool must be capable of solving OPFs of conventional AC systems.
2) The tool mustbe able to handle linear constraints of the state variables (to include constraints (33)).
3) The tool must have the possibility of using scripts (to implement the proposed algorithm described in sections IV-A and IV-B).

V. VALIDATION OF THE PROPOSED ALGORITHM IN 5-BUS STAGG'S TEST SYSTEM

To start with, the OPF algorithm proposed in Section IV (type 3), implemented in Matpower, has been validated against two OPF algorithms of type 1 and 2 already published in the literature. Type-1 models were used in [13] and were coded with GAMS [48]. Meanwhile, type-2 models were used in [17] with AIMMS [49].

The test case used for the validation is shown in Fig. 7, which correspond to cases `case5_stagg.m` (AC grid) and `case5_stagg_MTDCslack.m` (DC grid) of MatACDC. Total losses of the system are the objective function of the problem to be minimised. Constraints of the AC system are detailed in Tables I-II. Data of the VSC stations and the DC grid are provided in Table III.

Models type-1 and type-3 use (11) to compute converter losses, while model type-2 represents losses at each VSC station as a shunt conductance at the DC side, proportional to the square of the converter current [17] given by (16). For comparison purposes, loss coefficients of (11) and (16) have been adjusted to obtain 1 % losses at full load of the VSCs (Table III).

Results of the OPF problem obtained with each approach are compared in Tables IV-VI. Results obtained with the three models are almost the same. Total losses obtained with the three models are 4.14 MW. Results obtained with model type-2 differ slightly from the results obtained with modelstype-1 and type-3, due to the different model used for the converter losses.
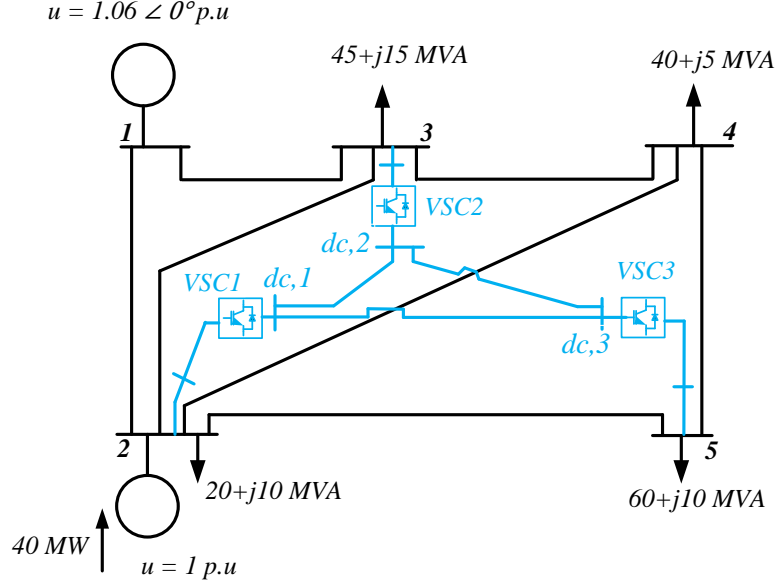
Fig. 7: 5-bus Stagg's test system with an embedded VSC-MTDC, used for comparison of OPF results.

TABLE I: 5-bus Stagg's system + VSC-MTDC. Generator constraints.

Gen	P_G^{max}/P_G^{min} (MW)	Q_G^{max}/Q_G^{min} (MVAr)
Gen1	250.00 / 10.00	100.00 / -100.00
Gen2	40.00 / 0.00	40.00 / -40.00

TABLE II: 5-bus Stagg's system + VSC-MTDC. AC-grid constraints. Nominal voltage of the AC grid: 345 kV.

AC bus	V^{max}/V^{min} (p.u)
$i = 1, 2$	1.02 / 1.00
$i = 3, 4, 5$	1.10 / 0.90
AC lines	$I_{ij}^{max} = 1.00$ p.u (rating of the line)

TABLE III: 5-bus Stagg's system + VSC-MTDC. Converter and DC grid parameters

Parameters Converter rating are base values for p.u.	Values
Rating VSC, DC voltage	100 MVA, ±345 kV
Configuration	Symmetrical monopole
Max. active (reactive) power	±100 MW (±100 MVAr)
Max. current	1 p.u
Max. DC voltage ($V_{dc,i}^{max}$ / $V_{dc,i}^{min}$)	1.10 / 0.90 p.u
Max. modulation index (m_i^{max})	1.22 p.u
Connection imp. ($\bar{Z}_{s,i} = R_{s,i} + jX_{s,i}$) (345/345 kV transformer)	$0.0016 + j0.2764$ p.u
VSCs' loss coefficients (models 1 and 3)	$a_i = b_i = 0$ and $c_i = 0.01$ p.u
VSCs' loss coefficient (in model 2)	$G_{0,i} = 0.01$ p.u
DC-line series resistance ($R_{dc,ij}$) lines 1-2 and 2-3 line 1-3	0.0520 p.u 0.0365 p.u
$V_{dc,i}^{max}$ / $V_{dc,i}^{min}$ (VSC2, DC slack)	1.02 / 1.02 p.u

TABLE IV: 5-bus Stagg's system + VSC-MTDC. Comparison of OPF results. AC buses and generators.

	Type 1 ([13])		Type 2 ([17])		Type 3 (proposed)	
bus	V (p.u)	θ (deg)	V (p.u)	θ (deg)	V (p.u)	θ (deg)
1	1.020	0.00	1.020	0.00	1.020	0.00
2	1.006	-3.15	1.006	-3.15	1.006	-3.15
3	0.992	-4.92	0.992	-4.92	0.992	-4.92
4	0.991	-5.28	0.991	-5.29	0.991	-5.28
5	0.991	-5.48	0.991	-5.49	0.991	-5.48
Gen	P_G (MW)	Q_G (Mvar)	P_G (MW)	Q_G (Mvar)	P_G (MW)	Q_G (Mvar)
1	129.14	-8.37	129.14	-8.38	129.14	-8.37
2	40.00	15.00	40.00	15.09	40.00	15.00

TABLE V: 5-bus Stagg's system + VSC-MTDC. Comparison of OPF results. Converters.

	Type 1 ([13])	Type 2 ([17])	Type 3 (proposed)
VSC	1, 2, 3	1, 2, 3	1, 2, 3
AC bus	2, 3, 5	2, 3, 5	2, 3, 5
P_s (MW)	-37.88, 12.54, 24.86	-37.55, 12.34, 24.72	-37.90, 12.54, 24.86
Q_s (MVAr)	0.00, 9.07, 6.16	0.00, 9.02, 6.12	0.00, 9.07, 6.16
V_s (p.u)	1.006, 0.992, 0.991	1.006, 0.992, 0.991	1.006, 0.992, 0.991
δ_s (deg)	-3.15, -4.92, -5.48	-3.15, -4.92, -5.49	-3.15, -4.92, -5.48
P_c (MW)	-37.88, 12.55, 24.87	-37.53, 12.34, 24.73	-37.87, 12.55, 24.87
Q_c (MVAr)	3.93, 9.74, 8.01	3.85, 9.68, 7.98	3.93, 9.74, 8.01
E_c (p.u)	1.010, 1.019, 1.011	1.010, 1.018, 1.011	1.010, 1.019, 1.011
δ_c (deg)	-9.07, -2.96, -1.55	-9.01, -3.00, -1.58	-9.07, -2.96, -1.55
m (p.u)	0.995, 1.009, 1.003	0.995, 1.008, 1.003	0.995, 1.009, 1.003

TABLE VI: 5-bus Stagg's system + VSC-MTDC. Comparison of OPF results. DC grid.

	Type 1 ([13])		Type 2 ([17])		Type 3 (proposed)	
DC bus	V_{dc} (p.u)	P_{dc} (MW)	V_{dc} (p.u)	P_{dc} (MW)	V_{dc} (p.u)	P_{dc} (MW)
1	1.015	37.90	1.015	37.38	1.015	37.73
2	1.010	-12.54	1.010	-12.37	1.010	-12.57
3	1.008	-24.86	1.008	-24.80	1.008	-24.93
DC line	$P_{cc,ij}$ (MW)	$P_{cc,ji}$ (MW)	$P_{cc,ij}$ (MW)	$P_{cc,ji}$ (MW)	$P_{cc,ij}$ (MW)	$P_{cc,ji}$ (MW)
1-2	19.27	-19.18	19.07	-18.98	19.27	-19.18
1-3	18.46	-18.34	18.31	-18.20	18.46	-18.34
2-3	6.61	-6.60	6.61	-6.60	6.61	-6.60

Finally, the optimality of the solution obtained with the proposed OPF algorithm is investigated numerically. The optimal P and Q injections of the VSC stations ($P_{s,i}^*$ and $Q_{s,i}^*$, respectively) are perturbed as:

$$P_{s,i}^p = P_{s,i}^* + \Delta P_p \tag{36}$$

$$Q_{s,i}^p = Q_{s,i}^* + \Delta Q_p \tag{37}$$

where ΔP_p and ΔQ_p are the amplitudes of the perturbation for P and Q injections of the VSCs, respectively. Parameters ΔP_p and ΔQ_p are changed from -40 MVA to 40 MVA with a step of 1 MVA. An AC/DC power flow is run (with MatACDC) for each perturbed injections of the VSCs (36)-(37). VSC2 is the DC slack in the power-flow calculation. The perturbation on the active-power and reactive-power injections are analysed separately. Total losses obtained when perturbing P injections, ΔP_p, (and $\Delta Q_p = 0$) are plotted in Fig. 8. Meanwhile, total losses obtained when perturbing Q injections, ΔQ_p, (and $\Delta P_p = 0$) are plotted in Fig. 9. In addition, the relative difference of total losses in comparison with losses obtained in the optimal solution is also showed in Figs. 8 and 9 (for perturbation on P and Q injections, respectively). The relative difference (γ_{loss}) is defined as:

$$\gamma_{loss} = \frac{P_{tot,loss} - P_{tot,loss}^*}{P_{tot,loss}^*} \tag{38}$$

where $P_{tot,loss}$ are the total system losses and $P_{tot,loss}^*$ are the total system losses obtained in the solution of the OPF.

Results of Figs. 8 and 9 confirm that total losses increase as the optimal solution is perturbed and the error shows an upward trend as the amplitude of the perturbation increases.
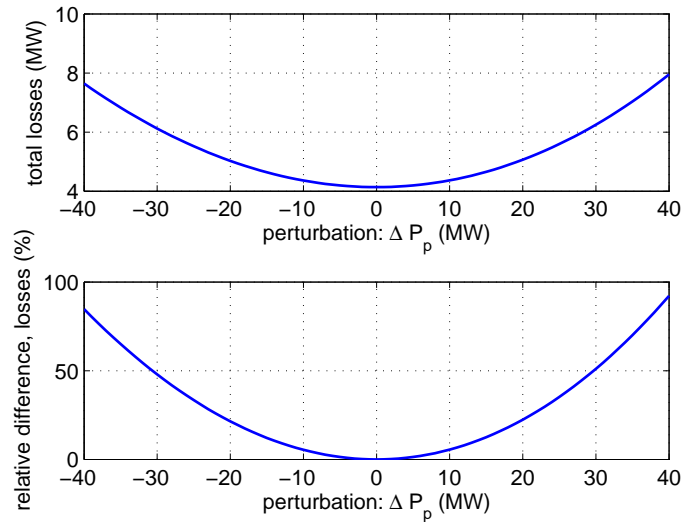

Fig. 8: 5-bus Stagg's system + VSC-MTDC. Total system losses obtained changing P injections of the OPF solution.
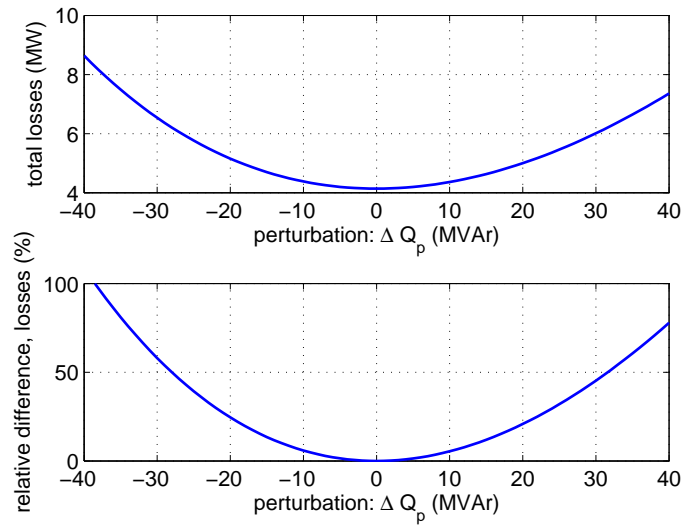

Fig. 9: 5-bus Stagg's system + VSC-MTDC. Total system losses obtained changing Q injections of the OPF solution.

VI. VALIDATION OF THE PROPOSED ALGORITHM IN IEEE 30-BUS TEST SYSTEM

Given the reduced size of the test system in Fig. 7, a larger system has also been used for validation, namely, the IEEE 30-bus test system [50] with two embedded VSC-MTDC systems, shown in Fig. 10. This test system was chosen because it is a typical IEEE benchmark, it was previously used in [4] with a type-1 model OPF approach and results could, therefore, be compared.
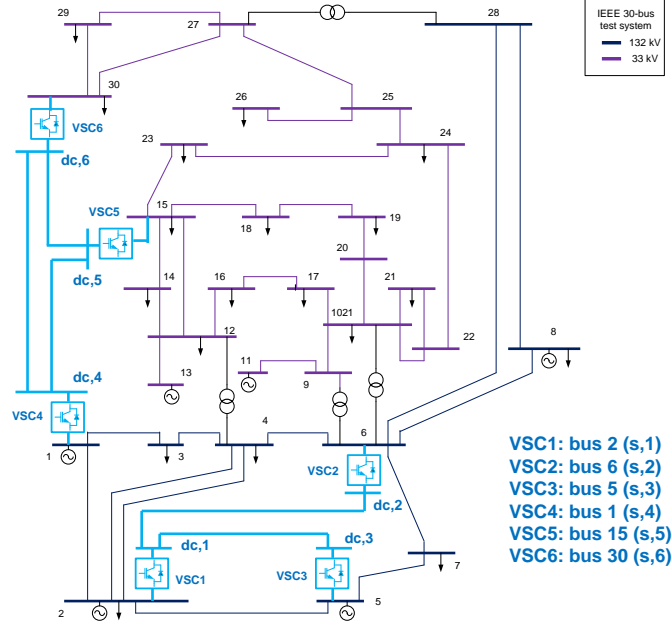

Fig. 10: IEEE 30-bus system + two VSC-MTDC systems [4].

Data of IEEE 30-bus test system can be found in [50]. Most data of the two embedded VSC-MTDC systems of Fig. 10 can be found in [4] and [51]. However, not all data are available in these references. Specifically,

- Values of connection impedances of the VSCs (phase reactor + transformer) are not provided.
- Values of resistances of the DC lines are not provided.
- Converter losses are assumed to be proportional to active-power injections of VSCs in [4]: $P_{loss,i} = \beta_i P_{c,i}$. However, values of coefficients β_i are not provided.

For the implementation of the test system of Fig. 10 in the proposed OPF model, these data related to the VSC-MTDC systems have been completed by assuming realistic values. Here, data for the OPF problem, including parameters provided in [4] and parameters which were assumed, are provided in tables VII-X, for completeness. It is worth pointing out that, in the proposed model, converter losses are represented by the quadratic function (12).

TABLE VII: IEEE 30-bus system + VSC-MTDCs. Generator constraints.

Gen	P_G^{max}/P_G^{min} (MW)	Q_G^{max}/Q_G^{min} (MVAr)
Gen1	160.00 / 0.00	100.00 / 0.00
Gen2	140.00 / 0.00	50.00 / -40.00
Gen5	40.00 / 0.00	40.00 / -40.00
Gen8	40.00 / 0.00	40.00 / -10.00
Gen11	30 .00/ 10.00	24.00 / -6.00
Gen13	30.00 / 0.00	24.00 / -6.00

TABLE VIII: IEEE 30-bus system + VSC-MTDCs. AC-grid constraints. Nominal voltage of the AC grid: 138 kV.

AC buses	$V^{max} = 1.06$ p.u., $/V^{min} = 0.94$ p.u
AC branches	$S_{ij}^{max} = 100$ MVA (rating of the branch)

TABLE IX: IEEE 30-bus system + VSC-MTDCs. Generation costs.

Gen	c_a (€)	c_b (€/MWh)	c_c (€/MW²h)
Gen1	0.00	20.00	0.00
Gen2	0.00	20.00	0.00
Gen5	0.00	40.00	0.00
Gen8	0.00	40.00	0.00
Gen11	0.00	40.00	0.00
Gen13	0.00	40.00	0.00

TABLE X: IEEE 30-bus system + VSC-MTDCs. Converter and DC grid parameters

Parameters Converter rating are base values for p.u.	Values
Rating VSC, DC voltage	100 MVA, ±320 kV
Configuration	Symmetrical monopole
Max. active (reactive) power	±100 MW (±100 MVAr)
Max. current	1 p.u
Max. DC voltage ($V_{dc,i}^{max}$ / $V_{dc,i}^{min}$)	1.06 / 0.94 p.u
Max. active power, DC lines ($P_{cc,ij}^{max}$)	100 MW
Max. modulation index (m_i^{max})	1.19 p.u
Connection imp. ($\bar{Z}_{s,i} = R_{s,i} + jX_{s,i}$) (VSCs 1, 2, 3, 4: 330/132 kV transformer) (VSCs 5, 6: 330/33 kV transformer)	$0.00 + j0.30$ p.u
VSCs' loss coefficients	$a_i = 2 \times 10^{-3}$, $b_i = 8 \times 10^{-3}$ and $c_i = 6 \times 10^{-3}$ p.u
DC-line series resistance ($R_{dc,ij}$)	0.005 p.u

Tables XII and XII compare the OPF results obtained with the proposed model (type-3), implemented in Matpower, with the ones obtained in [4] (type-1), implemented in GAMS. Variables which were not provided in [4] are left in blank. Results show good agreement: active-power injections of generators and VSCs obtained with both models are very close. Reactive-power injections of generators and VSCs match in almost all cases. However, it should be highlighted that reactive-power injections in some generators and VSCs present important differences (Generator 5, VSC 3 and VSC 4). This is due to the difference in parameters of the test system which were assumed in the proposed model (connection impedances of the VSCs, resistances of DC lines and coefficients of converter losses), and also due to the different converter-loss models. For example, VSC 4 is placed at the same bus of Generator 1 and, therefore, the relevant Q injection for the OPF solution is the net Q injection at the bus (Generator 1 + VSC 4). Since the model for converter losses in [4] is proportional to the P injection of the VSC, an additional Q injection in the converter, it does not produce additional losses. However, since the model for converter losses in the OPF algorithm proposed in this work depends on the converter current (12), an additional Q injection produces additional losses and the OPF algorithm should move any Q injection to the synchronous generator, instead of using the VSC. This means that, in the OPF solution of the latter, Generator 1 produces more reactive power than VSC 4. This result is consistent with the findings in [13] where the impact of converter losses on OPF solutions was highlighted. All variables of the VSC stations obtained with the proposed model are shown in Table XIII.

Finally, the optimality of the solution obtained with the proposed OPF algorithm in the test system of Fig. 10 is proved numerically. The optimal P and Q injections of the VSC stations ($P_{s,i}^*$ and $Q_{s,i}^*$, respectively) were perturbed as in the previous section (see (36)-(37)). Parameters ΔP_p and ΔQ_p were changed from -20 MVA to 20 MVA with a step of 1 MVA. An AC/DC power flowwas run (with MatACDC) for each pair of perturbedP & Q injections of the VSCs (36)-(37). VSC1 and VSC4 where set as DC slack converters of the two VSC-MTDC systems of Fig. 10, for power-flow calculation. Total operating costs obtained for each perturbation on the P injections, ΔP_p, (and $\Delta Q_p = 0$) are showed in the upper plot of Fig. 11. Meanwhile, total operating costs obtained for each perturbation on the Q injections, ΔQ_p, (and $\Delta P_p = 0$) are showed in the lower plot Fig. 11.

Results of Fig. 11 confirm that total system operating costs increase as the optimal solution is perturbed. Therefore, the proposed OPF algorithm obtains the optimal solution of the hybrid AC/DC system successfully.

TABLE XI: IEEE 30-bus system + VSC-MTDCs. Comparison of OPF results. AC generators.

	Type 1 ([4])		Type 3 (proposed)	
Operating cost €/h	5808.80		5822.80	
Gen	P_G (MW)	Q_G (MVAr)	P_G (MW)	Q_G (MVAr)
Gen1	150.44	0.00	151.14	0.00
Gen2	140.00	4.72	140.00	5.66
Gen5	0.00	6.24	0.00	23.23
Gen8	0.00	27.62	0.00	28.04
Gen11	0.00	9.53	0.00	9.80
Gen13	0.00	12.43	0.00	13.02

TABLE XII: IEEE 30-bus system + VSC-MTDCs. Comparison of OPF results. VSCs and DC grid.

	Type 1 ([4])		Type 3 (proposed)	
VSC	P_c (MW)	Q_c (MVAr)	P_c (MW)	Q_c (MVAr)
1	-79.96	17.31	-79.56	17.43
2	25.74	2.68	23.38	1.63
3	52.53	26.89	54.83	8.34
4	-59.91	-17.45	-58.78	1.71
5	40.44	10.07	40.92	12.98
6	18.45	3.49	16.77	0.98
DC bus	V_{dc} (p.u)	P_{dc} (MW)	V_{dc} (p.u)	P_{dc} (MW)
1	1.060	-	1.060	79.05
2	1.050	-	1.059	-23.66
3	1.040	-	1.057	-55.23
4	1.060	-	1.060	58.37
5	1.050	-	1.058	-41.26
6	1.050	-	1.059	-17.02
DC line	$P_{cc,ij}$ (MW)	$P_{cc,ji}$ (MW)	$P_{cc,ij}$ (MW)	$P_{cc,ji}$ (MW)
1-2	-	-	23.68	-23.66
1-3	-	-	55.36	-55.23
4-5	-	-	33.23	-33.18
4-6	-	-	25.14	-25.11
5-6	-	-	-8.08	8.09

TABLE XIII: IEEE 30-bus system + VSC-MTDCs. OPF results obtained with the proposed model. Converters.

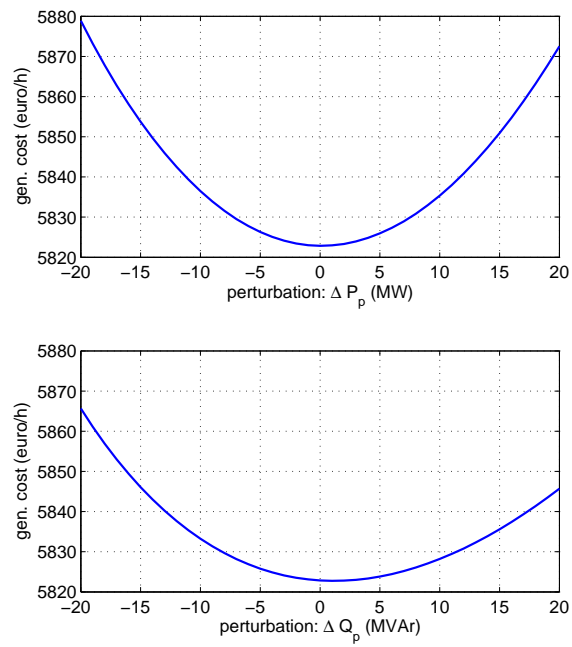| Converter	1	2	3	4	5	6
AC bus	2	6	5	1	15	30
P_s (MW)	-80.14	23.33	54.55	-59.10	40.76	16.74
Q_s (MVAr)	0.00	0.12	0.00	-7.78	8.27	0.18
V_s (p.u)	1.052	1.038	1.035	1.060	1.049	1.060
δ_s (deg)	-1.66	-4.52	-5.74	0.00	-5.57	-4.60
P_c (MW)	-79.56	23.38	54.83	-58.78	40.92	16.77
Q_c (MVAr)	17.43	1.63	8.34	1.71	12.98	0.98
E_c (p.u)	1.069	1.042	1.052	1.046	1.083	1.063
δ_c (deg)	-14.02	-0.81	2.91	-9.17	0.56	-2.05
m (p.u)	1.009	0.984	0.995	0.987	1.024	1.004
P_{loss} (MW)	0.51	0.28	0.40	0.42	0.35	0.25

Fig. 11: IEEE 30-bus system + VSC-MTDCs. Operating cost obtained changing P injections only (upper plot) and Q injections only (lower plot) of the OPF solution.

VII. Additional Case study

The use of the OPF algorithm proposed in Section IV (type 3), implemented in Matpower, is further illustrated in the Cigré Nordic32A system with an embedded VSC-MTDC system, similar to the one used in [52].This system, depicted in Fig. 12, has heavy power flows from the north and south parts to the central one and it is an attractive problem to be tackled with HVDC-VSC technology. All data of the AC system can be found in [53], [54] and a comprehensive description of the system can be found in [55]. AC-voltage limits are set to $\pm$ 7 % and upper bound of the magnitude of the current through AC lines is set to their thermal limits. Data of the VSC-MTDC system to be used here are provided in Table XIV. Rating values of VSC stations were chosen similar to the ones used in [56].
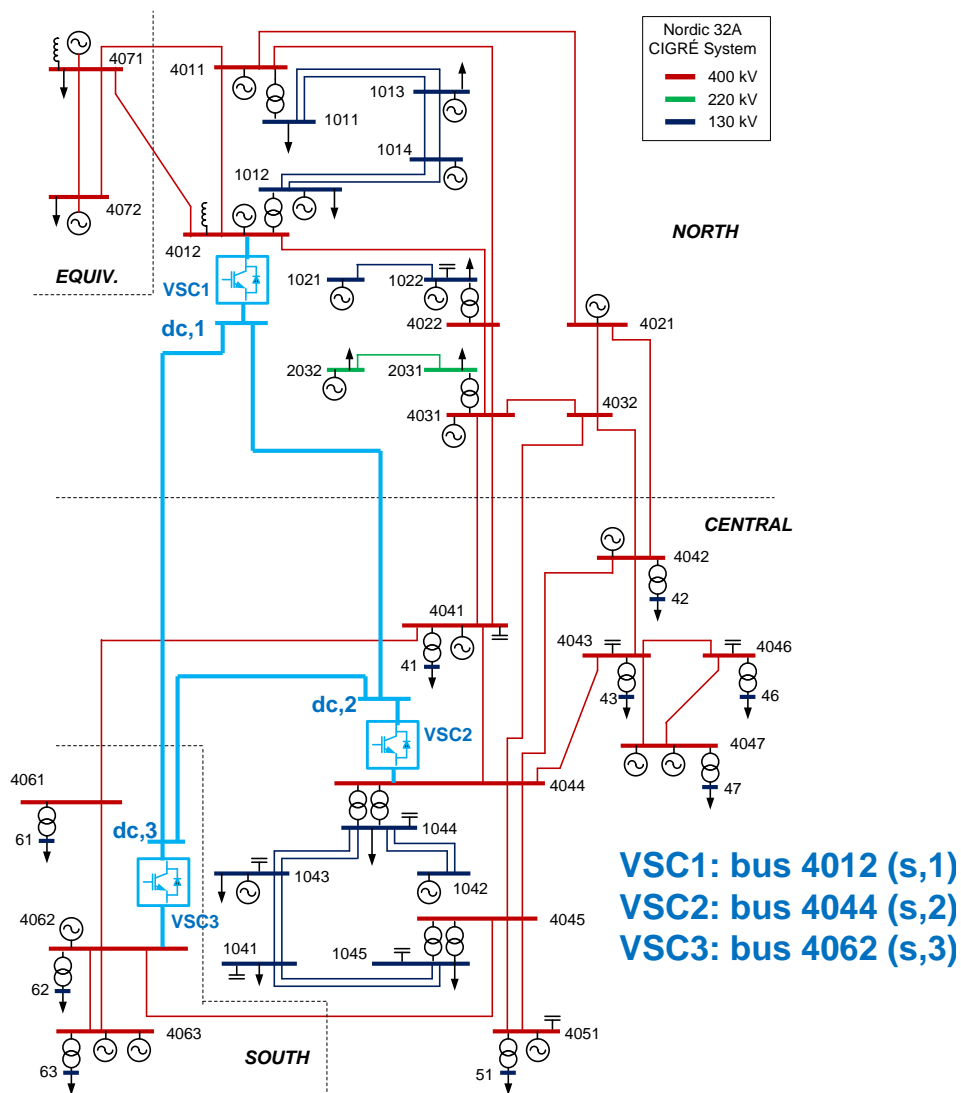

Fig. 12: Nordic 32A system + a VSC-MTDC system.

A. Minimisation of generation costs

Total generation cost is used as the objective function of the OPF. Coefficients of the generation-cost function have been obtained from Table IV of [7]. An OPF using the proposed algorithm has been run and results are shown in Tables XV-XVI. The optimal solution is when the VSC-MTDC system carries a large amount of active power from the northern area to the southern area (from VSC1 to VSC3). This is due to the fact that the North has cheaper generation. The biggest consumption points are located in the central area. The VSC-MTDC transmits

17

TABLE XIV: Nordic 32A system + VSC-MTDC. Converter and DC grid parameters

Parameters Converter rating are base values for p.u.	Values
Rating VSC, DC voltage	1000 MVA, $\pm$320 kV
Configuration	Symmetrical monopole
Max. active (reactive) power	$\pm$1000 MW ($\pm$450 MVAr)
Max. current	1 p.u
Max. DC voltage ($V_{dc,i}^{max}$ / $V_{dc,i}^{min}$)	1.07 / 0.93 p.u
Max. modulation index (m_i^{max})	1.19p.u
Connection imp. ($Z_{s,i} = R_{s,i} + jX_{s,i}$) (400/330 kV transformer)	0.002 + j0.17 p.u
VSCs' loss coefficients (a/b) VSCs' loss coefficients (c_{rec}/c_{inv})	5.25/1.65 $\times10^{-3}$ p.u. 2.10/3.14 $\times10^{-3}$ p.u.
DC-line series resistance ($R_{dc,ij}$)	2.05 Ω
$V_{dc,i}^{max}$ / $V_{dc,i}^{min}$ (VSC2)	1.01 / 1.00 p.u

part of the generated active power to the Southern area, which switches off its expensive generation. The rest of the active power consumption in the central area is transmitted through the HVAC corridors. The operation cost in the optimal solution is 340,008.00 ($/h).

TABLE XV: Nordic 32A system + VSC-MTDC. OPF results. VSC stations.

Converter	1	2	3
AC bus	4012	4044	4062
P_s (MW)	-984.63	2.26	948.99
Q_s (MVAr)	106.54	299.58	12.74
V_s (p.u)	0.990	1.07	1.07
δ_s (deg)	-3.45	-67.66	-68.15
P_c (MW)	-983.03	2.39	950.25
Q_c (MVAr)	276.54	312.91	146.57
E_c (p.u)	1.021	1.118	1.084
δ_c (deg)	-12.99	-67.66	-60.15
m (p.u)	1.008	1.107	1.077
P_{loss} (MW)	10.05	5.88	8.37

TABLE XVI: Nordic 32A system + VSC-MTDC. OPF results. DC grid.

DC bus	V_{dc} (p.u) (p.u)	P_{dc} (MW)	DC line	$P_{dc,ij}$ (MW)	$P_{dc,ji}$ (MW)
1	1.013	-972.98	1-2	327.09	-326.05
2	1.010	8.27	1-3	645.89	-641.83
3	1.007	958.62	2-3	317.78	-316.79

The dispatch of generators and VSCs given by the OPF is compared with a base case, in which generators have the same data as the operating point described in [53] and power-flow calculation carried out with:

- VSC1: $P_{s,1} = -500$ MW, $Q_{s,1} = 0$ MVAr.
- VSC2: $P_{s,2} = 700$ MW, $Q_{s,2} = 0$ MVAr.
- VSC3: $V_{dc,3} = 1$ p.u, $Q_{s,3} = 0$ MVAr (DC slack).

Results obtained in the base case and by the optimal power flow algorithm are compared in Table XVII. In the OPF solution, operation costs are reduced from 463,461.00 ($/h) to 340,008.00 ($/h), by increasing the cheaper generation in the North, switching off reducing to zero the more expensive generation in the South and increasing the power-flow transfer from the northen to the southen areas through the VSC-MTDC system.

Finally, Table XVIII reports nodal marginal prices at a set of AC buses in North, Centre and South, as well as the nodal marginal prices at the AC and DC buses of the VSC stations (obtained from Matpower output). Nodal marginal price at one bus (λ_i) measures the increment of total generation cost (C_T, objective function) if the demand at that bus ($P_{D,i}$) increases 1 MW [57]:

$$\lambda_i = \frac{\partial C_T}{\partial P_{D,i}} \qquad (39)$$

TABLE XVII: Nordic 32A system + VSC-MTDC. OPF results (minimisation of the generation costs).

	Base Case	Optimal Solution A
Operation costs ($/h)	463461	340008
Generation / Load (MW)		
North	6927.40 / 900.00	8694.20 / 900.00
Centre	2850.00 / 6350.00	2880.30 / 6350.00
South	1590.00 / 1390.00	0.00 / 1390.00
P / Q of the VSCs ($P_{s,i}$ (MW) / $Q_{s,i}$ (MVAr))		
VSC1	-500.00 / 0.00	-984.63 / 106.54
VSC2	700.00 / 0.00	2.26 / 299.58
VSC3	-223.97 / 0.00	948.99 / 12.51

Table XVIII shows that nodal marginal prices at buses located at the North (e.g. at bus 4011 and at AC bus of VSC1) are lower than the ones at the South (e.g. at buses 4043, 4063 and at AC buses of VSCs 2 and 3). This is because cheaper generation is located at the North. Nodal marginal prices at DC buses are close to 55 $/MW-h, including DC bus of VSC1, which is located at the North. The nodal marginal price at VSC1 is remarkable higher at its DC bus than at its AC bus because if demand at the DC bus increases, the increase in generation must supply the losses at the converter station, too. Notice, however, that nodal marginal prices at DC buses are for illustration purposes, since, typically, DC buses will not have demand.

TABLE XVIII: Nordic 32A system + VSC-MTDC. OPF results. Nodal marginal prices.

Bus	λ_i ($/MW-h)
Bus 4011 (North)	32.16
Bus 4043 (Centre)	55.44
Bus 4063 (South)	57.36
VSC1, AC bus (4012)	32.43
VSC2, AC bus (4044)	55.59
VSC3, AC bus (4062)	56.47
VSC1, DC bus $(dc, 1)$	55.24
VSC2, DC bus $(dc, 2)$	55.59
VSC3, DC bus $(dc, 3)$	55.94

B. Minimisation of system losses

Another realistic application of OPF calculation is to minimise the total losses of the system, given a pre-defined generation dispatch (in practice, obtained from market rules). Therefore, in this case, P and Q injections of VSC stations and Q injections of generators are dipatched by the OPF, but P injections of generators are fixed. Therefore, the value of total losses of the system is used as objective function. The generation dispatch of the base case in Section VII-A is considered.

OPF results using the proposed algorithm are compared with the base case in Table XIX. The VSC-MTDC system transmits the active power from the North (VSC1) to the Centre (VSC2), reducing the total losses from 321.12 MW to 250.81 MW.

TABLE XIX: Nordic 32A system + VSC-MTDC. OPF results (minimisation of the system losses).

	Base Case	Optimal Solution B
Total losses (MW)	321.12	250.81
Generation / Load (MW)		
North	6927.40 / 900.00	6750.81 / 900.00
Centre	2850.00 / 6350.00	2850.00 / 6350.00
South	1590.00 / 1390.00	1590.00 / 1390.00
P / Q of the VSCs ($P_{s,i}$ (MW) / $Q_{s,i}$ (MVAr))		
VSC1	-500.00 / 0.00	-966.58 / 50.00
VSC2	700.00 / 0.00	998.45 / -90.61
VSC3	-223.97 / 0.00	-65.63 / -33.08

VIII. CONCLUSIONS

Although several OPF algorithms for AC/DC systems have been proposed in the past, the user has to code the whole model and power-flow equations of the system in most of them, without having the possibility of solving an OPF with a conventional only-AC OPF tool. This can be a problem in practice, since it would require the development of new models to be able to solve OPFs in AC/DC systems, only possible if the only-AC OPF tool is open source. In most commercial only-AC tools for power system analysis, the user can not change power-flow equations and, therefore, OPF in hybrid AC/DC systems cannot be carried out.

To tackle this obstacle, a simplified algorithm to solve optimal power flows in hybrid VSC-based AC/DC systems has been proposed, emphasising the possibility of using an OPF tool only valid for AC systems. The proposed algorithm combines two characteristics of two different types of models proposed in previous work: (a) each VSC station is modelled using two conventional AC generators (one for the AC side and another one for the DC side) coupled by a linear constraint to ensure energy conservation in the VSC station and (b) DC grids are modelled as notional AC grids (DC branches are modelled as conventional resistive AC branches, due to the equivalence of their power-flow equations, in p.u.). Therefore, in the proposed approach, a VSC-based AC/DC system is transformed into an equivalent AC system, which can be plugged into a conventional only-AC tool to solve and OPF.

The proposed algorithm has been validated against two OPF algorithms proposed previously for AC/DC systems, showing good agreement. Results obtained in Cigré Nordic32A test system with an embedded multi-terminal VSC-HVDC systems have illustrated the potential of the proposed OPF approach. Results show that OPF problems in hybrid AC/DC systems can be tackled starting from available only-AC case studies with the addition of a DC plug-in.

Results have shown that generation costs or system losses can be reduced significantly by manipulating the opreating point of a VSC-MTDC system embedded in a meshed HVAC grid.

APPENDIX: AC/DC PER UNIT SYSTEM USED

The per-unit (p.u) system for AC/DC grids used in this work has followed the guidelines presented in [58]. The AC systems use the traditional three-phase p.u. system: a power base value ($S_{ac,B}$) and an AC-voltage base value (phase to phase) ($V_{ac,B}$).

The DC p.u. base values are defined as:

- Power base value: $S_{dc,B} = S_{ac,B}$.
- DC-voltage base value (pole to ground): $V_{dc,B}$.
- Current ($I_{dc,B}$) and impedance ($Z_{dc,B}$) base values:

$$I_{dc,B} = \frac{S_{dc,B}}{2V_{dc,B}}, \quad Z_{dc,B} = \frac{2V_{dc,B}^2}{S_{dc,B}}. \tag{40}$$

Using this p.u. system, the steady-state equations of a symmetrical monopolar HVDC link (Fig. 13), are:

$$V_{dc,1} - V_{dc,2} = R_{dc,12}I_{cc,12} \text{ (real)} \iff V_{dc,1} - V_{dc,2} = R_{dc,12}I_{cc,12} \text{ (p.u)} \tag{41}$$

$$P_{cc,12} = 2V_{dc,1}I_{cc,12} \text{ (real)} \iff P_{cc,12} = V_{dc,1}I_{cc,12} \text{ (p.u)} \tag{42}$$

where $V_{dc,i}$ is the voltage at DC bus i (pole to ground), $P_{cc,ij}$ is the total power leaving DC line ij (through both poles), $I_{cc,ij}$ is the current through DC line ij (through each pole) and $R_{dc,ij}$ is the resistance of DC line ij (of each pole).
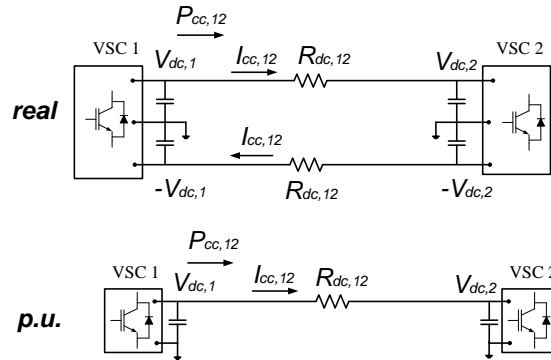

Fig. 13: Steady-state equivalent circuit of a DC line.

REFERENCES

[1] F. Capitanescu, "Critical review of recent advances and further developments needed in AC optimal power flow," *Electric Power Systems Research*, vol. 136, pp. 57–68, 2016.

[2] E. Bompard, G. Fulli, M. Ardelean, and M. Masera, "It's a Bird, It's a Plane, It's a... Supergrid," *IEEE power & energy magazine*, vol. 12, no. 2, pp. 41–50, 2014.

[3] B. Kazemtabrizi, "Mathematical Modelling of Multi-terminal VSC-HVDC links in Power Systems using Optimal Power Flows," PhD thesis, Department of Electronics and Electrical Engineering, University of Glasgow, UK, 2011.

[4] M. Baradar, M. Hesamzadeh, and M. Ghandhari, "Second-Order Cone Programming for Optimal Power Flow in VSC-Type AC-DC Grids," *IEEE Transactions on Power Systems*, vol. 28, no. 4, pp. 4282–4291, 2013.

[5] J. Cao, W. Du, H. F. Wang, and S. Q. Bu, "Minimization of Transmission Loss in Meshed AC/DC Grids With VSC-MTDC Networks," *IEEE Transactions on Power Systems*, vol. 28, no. 3, pp. 3047–3055, 2013.

[6] M. Vrakopoulou, S. Chatzivasileiadis, E. Iggland, M. Imhof, T. Krause, O. Makela, J. L. Mathieu, L. Roald, R. Wiget, and G. Andersson, "A Unified Analysis of Security-Constrained OPF Formulations Considering Uncertainty, Risk, and Controllability in Single and Multi-area Systems," *Proc. Bulk Power System Dynamics and Control - IX Optimization, Security and Control of the Emerging Power Grid Symposium (IREP)*, 2013, pp. 1–19.

[7] W. Feng, L. A. Tuan, L. B. Tjernberg, A. Mannikoff, and A. Bergman, "A New Approach for Benefit Evaluation of Multiterminal VSCHVDC Using A Proposed Mixed AC/DC Optimal Power Flow," *IEEE Transactions on Power Systems*, vol. 29, no. 1, pp. 432–443, 2014.

[8] E. Iggland, R. Wiget, S. Chatzivasileiadis, and G. Anderson, "Multi-Area DC-OPF for HVAC and HVDC Grids," *IEEE Transactions on Power Systems*, vol. 30, no. 5, pp. 2450–2459, 2015.

[9] M. Aragues-Penalba, J. Beerten, J. Rimez, D. Van Hertem, and O. Gomis-Bellmunt, "Optimal power flow tool for hybrid AC/DC systems," *Proc. 11th IET International Conference on AC and DC Power Transmission, Birmingham, UK*, 2015 pp. 1–7.

[10] F. González-Longatt, "Optimal Steady-State Operation of a MTDC system based on DC-Independent System Operator Objectives," *Proc. 11th IET International Conference on AC and DC Power Transmission, Birmingham, UK*, 2015 pp. 1–7.

[11] J. Rimez and R. Belmans, "A combined AC/DC optimal power flow algorithm for meshed AC and DC networks linked by VSC converters," *International Transactions on Electrical Energy Systems*, vol. 25, pp. 2024–2035, 2015.

[12] R. Teixeira Pinto, M. Aragues-Penalba, O. Gomis-Bellmunt, and A. Sumper, "Optimal Operation of DC Networks to Support Power System Outage Management," *IEEE Transactions on Smart Grid*, vol. 7, no. 6, pp. 2953–2961, 2016.

[13] Q. Zhao, J. García-González, O. Gomis-Bellmunt, E. Prieto-Araujo, and F. M. Echavarren, "Impact of converter losses on the optimal power flow solution of hybrid networks based on VSC-MTDC," *Electric Power Systems Research*, vol. 151, pp. 395–403, 2017.

[14] Z. Yang, H. Zhong, A. Bose, Q. Xia, and C. Kang, "Optimal Power Flow in AC-DC Grids with Discrete Control Devices," *IEEE Transactions on Power Systems*, vol. 33, no. 2, pp. 1461–1472, 2018.

[15] M. Aragues-Penalba, A. Egea-Alvarez, S. Galceran Arellano, and O. Gomis-Bellmunt, "Droop control for loss minimization in HVDC multi-terminal transmission systems for large offshore wind farms," *Electric Power Systems Research*, pp. 48–55, 2014.

[16] L. Hǎlibasić, S. Chatzivasileiadis, and P. Pison, "Coordinating Flexibility under Uncertainty in Multi-Area AC and DC Grids," *Proc. IEEE/PES PowerTech, Manchester, UK*, 2017, pp. 1–7.

[17] A. A. Ibrahim, B. Kazemtabrizi, and C. Dent, "Operational planning and optimisation in active distribution networks using modern intelligent power flow controllers," *Proc. IEEE/PES Innovative Smart Grid Technologies Conference Europe (ISGT), Ljubljana, Slovenia*, 2016, pp. 1–6.

[18] S. Chatzivasileiadis, T. Krause, and G. Andersson, "Security-Constrained Optimal Power Flow including Post-Contingency Control of VSC-HVDC lines," *Proc. XII Symposium of Specialists in Electrical Operation and Expansion Planning (SEPOPE), Rio de Janeiro, Brasil*, 2012, pp. 1–12.

[19] R. Wiget, E. Iggland, and G. Andersson, "Security Constrained Optimal Power Flow for HVAC and HVDC Grids," *Proc. Power Systems Computation Conference (PSCC), Wroclaw, Poland*, 2014, pp. 1–7.

[20] J. Cao, W. Du, and H. F. Wang, "An Improved Corrective Security Constrained OPF for Meshed AC/DC Grids With Multi-Terminal VSC-HVDC," *IEEE Transactions on Power Systems*, vol. 31, no. 1, pp. 485–495, 2016.

[21] T. Sennewald, T. Sass, and D. Westermann, "A preventive security constrained optimal power flow for mixed AC-HVDC-systems," *Proc. 13th IET International Conference on AC and DC Power Transmission, Manchester, UK*, 2017, pp. 1–7.

[22] E. Acha, B. Kazemtabrizi, and L. M. Castro, "A New VSC-HVDC Model for Power Flows Using the Newton-Raphson Method," *IEEE Transactions on Power Systems*, vol. 28, no. 3, pp. 2602–2612, 2013.

[23] B. Kazemtabrizi and E. Acha, "An Advanced STATCOM Model for Optimal Power Flows Using Newton's Method," *IEEE Transactions on Power Systems*, vol. 29, no. 2, pp. 514–525, 2014.

[24] E. Acha and L. M. Castro, "A generalized frame of reference for the incorporation of multi-terminal VSC-HVDC systems in power flow solutions," *Electric Power Systems Research*, vol. 136, pp. 415–424, 2016.

[25] Siemens PTI, *PSS/E 32.0.5 Users Manual*, 2010.

[26] DigSILENT, *PowerFactory 2017 User Manual*, 2017.

[27] G. Daelemans, K. Srivastava, M. Reza, S. Cole, and R. Belmans, "Minimization of steady-state losses in meshed networks using VSC HVDC," *Proc. IEEE/PES General Meeting, Calgary, AB, Canada*, 2009, pp. 1–5.

[28] E. Acha, C. R. Fuerte-Esquivel, Ambriz-Pérez, and C. Angeles-Camacho, *FACTS: modelling and simulation in power networks*. Chinchester, England, John Wiley & Sons, 2004.

[29] K. Sharifabadi, L. Harnefors, N. Hans-Peter, S. Norrga, and R. Teodorescu, *Design, Control, and Application of Modular Multilevel Converters for HVDC Transmission Systems*. Chinchester, England, John Wiley & Sons, 2016.

[30] C. Angeles-Camacho, O. L. Tortelli, E. Acha, and C. R. Fuerte-Esquivel, "Detailed and Averaged Models for a 401-Level MMCHVDC System," *IEE Proceedings - Generation, Transmission and Distribution*, vol. 150, no. 6, pp. 691–696, 2003.

[31] A. Pinzano-Martinez, C. R. Fuerte-Esquivel, H. Ambriz-Pérez, and E. Acha, "Detailed and Averaged Models for a 401-Level MMCHVDC System," *IEEE Transactions on Power Systems*, vol. 22, no. 4, pp. 1794–1803, 2007.

[32] X.-P. Zhang, "Multiterminal Voltage-Sourced Converter-Based HVDC Models for Power Flow Analysis," *IEEE Transactions on Power Systems*, vol. 19, no. 4, pp. 1877–1884, 2004.

[33] L. Gengyin, Z. Ming, H. Jie, L. Guangkai, and L. Haifeng, "Power flow calculation of power systems incorporating vsc-hvdc," *Proc. International Conference on Power System Technology (POWERCON), Singapore,*, vol. 2, 2004, pp. 1562–1566.

[34] Q. Chen, T. Q. Tang, and W. Xu, "AC-DC power flow algorithm for multi-terminal VSC-HVDC systems," *Electric Power Automation Equipment*, vol. 25, no. 6, pp. 2602–2612, 2005.

[35] J. Beerten, S. Cole, and R. Belmans, "A sequential AC/DC power flow algorithm for networks containing Multi-terminal VSC HVDC systems," *Proc. IEEE/PES General Meeting, Minneapolis, USA*, 2010, pp. 1–7.

[36] T. M. Haileselassie and K. Uhlen, "Power Flow Analysis of Multi-terminal HVDC Networks," *Proc. IEEE/PES PowerTech Conference, Trondheim, Norway*, pp. 1–6, 2011.

[37] F. Ye, Z. N. Wei, and G. Q. Sun, "Improved Power Flow Algorithm Incorporating Multi-Terminal VSC-HVDC," *Advanced Materials Research*, vol. 383-390, pp. 2188–2194, 2011.

[38] J. Beerten, S. Cole, and R. Belmans, "Generalized Steady-State VSC MTDC Model for Sequential AC/DC Power Flow Algorithms," *IEEE Transactions on Power Systems*, vol. 27, no. 2, pp. 821–829, 2012.

[39] F. Gonzalez-Longatt, J. M. Roldan, and C. A. Charalambous, "Solution of AC/DC Power Flow on a Multi- Terminal HVDC System: Illustrative Case Supergrid Phase I," in *Proc. Universities Power Engineering Conference (UPEC), London, UK*, 2012, pp. 1–6.

[40] W. Wang and M. Barnes, "Power Flow Algorithms for Multi-Terminal VSC-HVDC With Droop Control," *IEEE Transactions on Power Systems*, vol. 29, no. 4, pp. 1721–1730, 2014.

[41] R. Teixeira Pinto, C. Leon-Ramirez, M. Aragues-Penalba, A. Sumper, and E. Sorrentino, "A fast methodology for solving power flows in hybrid ac/dc networks: The European North Sea Supergrid case study," *Proc. International Exhibition and Conference for Power Electronics, Intelligent Motion, Renewable Energy and Energy Management (PCIM Europe), Nuremberg, Germany*, 2016, pp. 1–8.

[42] R. Chai, B. Zhang, J. Dou, Z. Hao, and T. Zheng, "Unified Power Flow Algorithm Based on the NR Method for Hybrid AC/DC Grids Incorporating VSCs," *IEEE Transactions on Power Systems*, vol. 31, no. 6, pp. 4310–4318, 2016.

[43] J. C. Fernández-Pérez, F. M. Echavarren, and L. Rouco, "On the convergence of the sequential power flow for multiterminal VSC AC/DC systems," *IEEE Transactions on Power Systems*, vol. 33, no. 4, pp. 1–9, 2017.

[44] E. Acha and B. Kazemtabrizi, "A new STATCOM model for power flows using the NewtonRaphson method," *IEEE Transactions on Power Systems*, vol. 28, no. 3, pp. 2455–2465, 2013.

[45] R. D. Zimmerman, C. E. Murillo-Sánchez, and R. J. Thomas, "MATPOWER: Steady-State Operations, Systems Research and Education," *IEEE Transactions on Power Systems*, vol. 26, no. 1, pp. 12–19, 2011.

[46] ——, "MATPOWER's extensible optimal power flow architecture," *Proc. IEEE/PES General Meeting, Calgary, AB, Canada*, 2009, pp. 1–7.

[47] J. Beerten and R. Belmans, "Development of an open source power flow software for high voltage direct current grids and hybrid AC/DC systems: MATACDC," *IET Generation, Transmission & Distribution*, vol. 9, no. 10, pp. 966–974, 2015.

[48] R. E. Rosenthal, *GAMS - A Users Guide*. GAMS Development Corporation, Washington, DC, USA, 2017.

[49] M. Roelofs and J. Bisschop, *AIMMS - The Users Guide*. AIMMS Inc., 2017.

[50] R. Christie, "Power Systems Test Case Archive," Online:Online: https://labs.ece.uw.edu/pstca/ (accessed 24-01-2019).

[51] B. Baradar, "On the Efficiency and Accuracy of Simulation Methods for Optimal Power System Operation," PhD thesis, School of Electrical Engineering, KTH Royal Institute of Technology in Stockholm, Sweden, 2015.

[52] R. Eriksson, "Coordinated Control of Multiterminal DC Grid Power Injections for Improved Rotor-Angle Stability Based on Lyapunov Theory," *IEEE Transactions on Power Delivery*, vol. 29, no. 4, pp. 1789–1797, 2014.

[53] M. Stubbe (Convener), "Long Term Dynamics Phase II," Cigré Task Force 38.02.08 - TB 102, Tech. Rep., 1995.

[54] B. Karlsson, "Comparison of PSSE & PowerFactory." Degree Project, Uppsala Universitet., 2013.

[55] T. Van Cutsem and L. Papangelis, "Description, Modeling and Simulation Results of a Test System for Voltage Stability Analysis," Université de Liège, Tech. Rep., 2014.

[56] J. Peralta, H. Saad, S. Dennetiere, J. Mahseredjian, and S. Nguefeu, "Detailed and Averaged Models for a 401-Level MMC-HVDC System," *IEEE Transactions on Power Delivery*, vol. 27, no. 3, pp. 1501–1508, 2012.

[57] F. C. Schweppe, M. C. Caramanis, R. D. Tabors, and R. E. Bohn, *Spot Pricing of Electricity*. Kluwer Academic Publishers, 1988.

[58] J. Beerten, "Modeling and Control of DC Grids," PhD thesis, Faculty of Engineering Science, Katholieke Universiteit Leuven, Belgium, 2013.